AIAA JOURNAL
Vol. 42, No. 12, December 2004

Active Stiffener Actuators for High-Precision Shape Control of Circular Plate Structure

Michael K. Philen* and K. W. Wang†
Pennsylvania State University, University Park, Pennsylvania 16802

Spaced-based adaptive optic systems have gained considerable attention within the past couple of decades. Achieving the increasingly stringent performance requirements for these systems is greatly hindered by strict weight restrictions, size limitations, and subjected hostile environments. There has been considerable attention in lightweight adaptive optics, where piezoelectric sheet actuators are directly attached on the back of optical mirrors to achieve a high-precision surface shape with minimum additional weight. In recent studies, it was discovered that the performance of the system could be further improved if the piezoelectric sheet actuator were decoupled in direction, meaning that the actuation in one of the two directions is eliminated. To realize the decoupling effect, the concept of utilizing the active stiffener for high-precision shape control is proposed and investigated in the study. The active stiffener is a stiffener-piezoceramic actuator pair that consists of an passive insert (stiffener) placed between the host structure and the active piezoelectric actuator. The basic premise is that the insert (stiffener) will reduce the action transmitted in one direction while allowing adequate action to transmit in the orthogonal direction. In this research, analytical and experimental efforts are carried out to examine the effect of the active stiffener actuators for shape control of circular plate structures. Analysis is performed on two large flexible circular plate structures, one having the direct attached actuators and the other utilizing the active stiffener actuators. It is shown that more reductions in the surface error can be achieved with the active stiffeners, as compared to systems with the direct attached actuators. It is illustrated that the direct attached actuators generate more localized deformation in the structure, whereas the decoupling capability of the active stiffener reduces the undesired localized deformation considerably. The experimental results verify the analytical predictions and clearly demonstrate the performance improvement of the active stiffener concept over the direct attached actuator.

Nomenclature

A	=	surface area of host structure
$\boldsymbol{B}_{\text{PZT}}$	=	nodal forcing influence matrix
$\boldsymbol{C}_{\text{host}}$	=	symmetric material stiffness matrix for the host structure
$\boldsymbol{C}^{E}_{\text{PZT}}$	=	symmetric material stiffness matrix for the piezoelectric ceramic at constant electrical field
$\boldsymbol{C}_{\text{stiff}}$	=	symmetric material stiffness matrix for the stiffener (insert)
$\boldsymbol{D}$	=	nodal degree of freedom vector
E_{loc}	=	local surface error on host structure
E_{RMS}	=	rms surface error of host structure
$\boldsymbol{E}_s$	=	vector of errors in vertical direction for surface nodes
$\boldsymbol{E}_3$	=	vector of applied electrical fields
E^i_3	=	applied electrical field for ith piezoelectric ceramic
$\boldsymbol{e}_{\text{PZT}}$	=	piezoelectric electromechanical coupling vector
J^a	=	optimal electrical fields objective function for analytical model
J^e	=	optimal voltages objective function for experimental model
J^t	=	trial function magnitude objective function
$\boldsymbol{K}$	=	system stiffness matrix
n_{el}	=	number of finite elements
$\boldsymbol{P}$	=	vector of nodal loads
$\boldsymbol{T}_s$	=	boolean weighting matrix for vertical surface displacements
V	=	element volume
$\boldsymbol{V}_{\text{PZT}}$	=	vector of applied voltages (experiment)
V_{PZT1}, V_{PZT2}, V_{PZT3}	=	applied voltage for each piezoelectric actuator (experiment)
$\boldsymbol{Y}$	=	desired surface shape
$\hat{\boldsymbol{Y}}$	=	surface shape after actuation of piezoceramics
$\tilde{\boldsymbol{Y}}$	=	approximated surface shape determined by trial functions
ε	=	strain field vector
η	=	trial function magnitude vector
Π_{host}	=	potential energy function for host structure
Π_{PZT}	=	potential energy function for piezoelectric ceramic
Π_{stiff}	=	potential energy function for stiffener (insert)
$\boldsymbol{\Phi}_{\text{PZT}}$	=	experimentally determined nodal-voltage influence matrix
$\boldsymbol{\Phi}_0$	=	matrix of trial functions
φ_{PZT1}, φ_{PZT2}, φ_{PZT2}	=	experimentally determined nodal-voltage influence vectors

Presented as Paper 2003-1636 at the AIAA/ASME/ASCE/AHS/ASC 44th Structures, Structural Dynamics, and Materials Conference, Norfolk, VA, 7–10 April 2003; received 15 July 2003; revision received 24 May 2004; accepted for publication 4 July 2004.

*Eastman Kodak Fellow, 157 Hammond Building, Structural Dynamics and Controls Laboratory; mphilen@psu.edu.

†William E. Diefenderfer Chaired Professor in Mechanical Engineering, 157E Hammond Building, Structural Dynamics and Controls Laboratory; kwwang@psu.edu.

Introduction

PROVIDING high-precision surfaces for antenna reflectors and space-based optical mirrors has been a challenging problem for designers. Space-based optical systems are ever increasingly being challenged with lighter, stiffer, and larger diameter optic requirements having greater dimensional stability, precision, and pointing accuracy. As a result, research into adaptive or smart optical systems has been heavily pursued in the past couple of decades. Adaptive optical systems have been successfully implemented in ground-based telescopes, but these systems are extremely heavy because of the required backbone structure and large number of actuators, and therefore do not lend them applicable for space systems. Recently there has been considerable attention in developing

lightweight adaptive optics for spaced-based platforms, such as the polyvinylidene fluoride (PVDF) membrane mirror system developed and tested by Wagner et al.[1] and Agnes and Wagner.[2] Other researchers have investigated directly attaching piezoelectric sheet actuators to the back of optical mirrors to achieve a high-precision surface shape with minimum additional weight. Kuo and Bruno,[3] Liu et al.[4] and Kapania et al.[5] are a few examples of researchers who investigated the performance of directly attached piezoelectric actuators on optical mirrors for shape control.

Philen and Wang[6] investigated the shape control performance of a large flexible circular plate structure having directly attached thin strip piezoelectric sheet actuators placed in the plate's radial and circumferential directions. The actuators placed in radial lines were termed radial actuators, and the actuators placed in circumferential lines were called circumferential actuators. In their paper, it was discovered that the performance of the system could be further improved if the piezoelectric actuator were directionally decoupled, meaning that the circumferential (radial) action of the radial (circumferential) actuators is eliminated while the radial (circumferential) action is maintained. This is because due to their thin width, the circumferential action of the radial actuators will not provide the necessary authority to control the lower-order deformations in the circumferential direction (low-order circumferential wave number in Zernike polynomial), but will "excite" the higher-order (uncontrolled) deformations in the circumferential direction (likewise with the circumferential actuators and radial deformations). Therefore, with direct attached actuators, the two-dimensional action increases the difficulty for one to achieve an ultra-high-precision performance.

Problem Statement, Research Objective and Approach Overview

As shown by Philen and Wang,[6] decoupling the actuator improves the performance of the system, but it requires a mechanism to reduce the transmitted actuation in one of the two directions. To achieve this goal and advance the state of the art, an active stiffener (AS) concept is proposed for decoupling the two-dimensional action of the piezoelectric actuator. The active stiffener is a stiffener-piezoceramic actuator pair that consists of a passive insert (stiffener) placed between the host structure and the active piezoelectric actuator as seen in Fig. 1. The basic premise is that the insert (stiffener) will reduce the transmitted moment to the host structure in the y direction (defined to be the decoupled direction) while allowing an adequate moment to transmit in the x direction (the actuation direction).

The objectives of this research are to 1) develop a well-integrated actuator-stiffener-structure model and investigate the stiffeners' decoupling effect, 2) examine the performance of the AS for shape control of a circular plate structure and compare with an equivalent structure having the direct attached (DA) actuators, and 3) experimentally validate the analytical prediction through evaluating the performance of both the direct attached actuators and the active stiffener actuators bonded to a flexible plate.

Previous investigations[7,8] have examined an active stiffener concept applying piezoelectric patches on the sides of structural stiffeners. The focus of those studies and the configuration of the stiffeners are different from what are being examined in this present research. In other words, these previous investigations were not concerned with the directional decoupling ability of the actuators and have disregarded the local deformations of the host structure between the stiffeners. These local deflections are crucial factors for high-precision shape control.

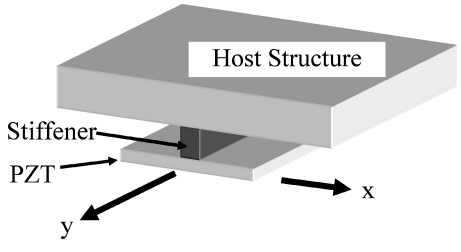

Fig. 1 Illustration of active stiffener concept.

For the analytical study, results are obtained through analysis on two three-dimensional solid finite element models of a large circular plate optical mirror structure (designated as large-scale analytical models), where the first plate has the active stiffener treatment and the second plate is applied with direct attached actuators. In this study, the mirror is limited to a surface mass less than 10 kg/m^2. The surface error is assumed to be in the form of the lower Zernike polynomials, and its primary contribution is from manufacturing errors, thermal loadings, and self-weight. Based on results from previous studies and preliminary investigations, the configuration of active stiffeners placed in both of the plate's radial and circumferential line directions are chosen to satisfy the strict weight restrictions and the properties of the Zernike polynomials. For shape control, a least-squares method is derived, which determines the optimal electrical fields for each actuator. The performance of the active stiffener for reduction of the surface error is then presented. Experimental results from two circular plates, one utilizing the direct attached actuators and the other using the active stiffener actuators, are presented afterwards. The analytical models of the two experimental plates are derived using the same finite element formulation as the large-scale analytical models and are referred to as the small-scale analytical models. Lastly, the experimental results are compared to the analytical results obtained from the small-scale analytical models.

Mathematical Formulation

Finite Element Model of Plate with Active Stiffeners (Large-Scale Analytical Models)

The potential energy for a linearly elastic body without an initial strain field, initial stresses, body forces, and surface tractions is defined as shown in Eq. (1):

$$\Pi = \int_V \left(\frac{1}{2}\varepsilon^T C\varepsilon\right) \mathrm{d}V - \boldsymbol{D}^T\boldsymbol{P} \tag{1}$$

For the host structure and stiffeners with no nodal loads, the potential energies are

$$\Pi_{\text{host}} = \int_V \left(\frac{1}{2}\varepsilon^T C_{\text{host}}\varepsilon\right) \mathrm{d}V \tag{2}$$

$$\Pi_{\text{stiff}} = \int_V \left(\frac{1}{2}\varepsilon^T C_{\text{stiff}}\varepsilon\right) \mathrm{d}V \tag{3}$$

For each piezoelectric actuator, the potential energy can be written as

$$\Pi_{\text{PZT}} = \int_V \left(\frac{1}{2}\varepsilon^T \boldsymbol{C}^E_{\text{PZT}}\varepsilon - \varepsilon^T \boldsymbol{e}_{\text{PZT}} E^i_3\right) \mathrm{d}V \tag{4}$$

The finite element model uses the familiar 20 noded quadratic "serendipity" solid isoparametric elements. A three-point Gauss quadrature is used for integration. For details regarding the derivations of the element and integration procedure, the reader is referred to Cook et al.[9]

Shown in Fig. 2 is the finite element model of the mirror with the active stiffeners. The figure reveals the top of the plate where a detailed cross-sectional view reveals the active stiffeners. The finite element model of the mirror with the direct attached actuators is shown in Fig. 3. The system parameters can be found in Table A1 in the Appendix. By taking advantage of the symmetry of the circular plate and the actuator configuration, it is possible to model the complete structure using only $\frac{1}{4}$ the plate. The boundary conditions are such that the center is fixed, and the symmetry condition forces the displacements along the sides to be equal to zero in the direction orthogonal to the free face (Figs. 2 and 3). Although the boundary

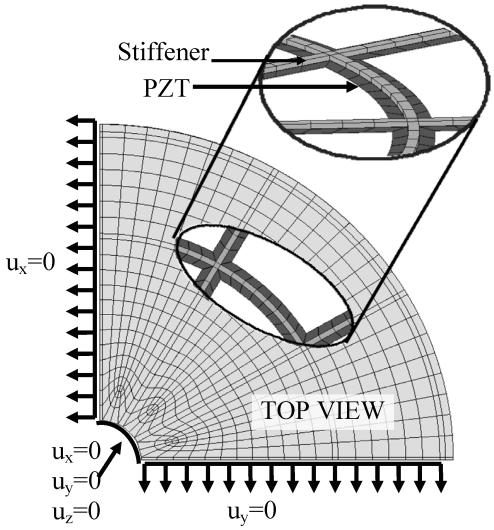

Fig. 2 Large-scale analytical model of active stiffener system with prescribed boundary conditions.

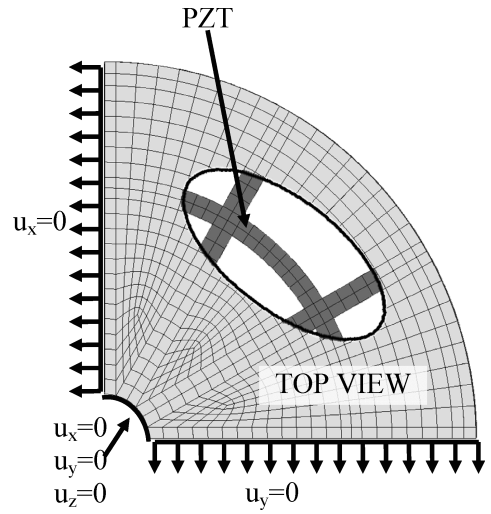

Fig. 3 Large-scale analytical model of direct attached system with prescribed boundary conditions.

conditions prevent nonsymmetric responses, the $\frac{1}{4}$-plate model is sufficient in providing an analysis for the illustration of the excitation of the higher-order deformations caused by the direct attached actuators and for comparing the shape control performance of the two actuation methods (direct attached and active stiffener).

For both systems, there are 42 total actuators with six actuators per radial line and nine per circumferential line, and the total mass for each system is kept equal to 50 kg. For a complete circular plate, the total number of actuators would be 144 using the same configuration. Each piezoelectric actuator has a thickness of 0.5 mm and a width of 76.2 mm, and the stiffeners are 13.8 mm in width with a height of 3.0 mm (see Fig. 4 for dimension definitions).

Optimal Electrical Fields for Shape Control

To determine the optimal electrical fields for each piezoelectric ceramic actuator to control the static shape of the mirror, a quadratic function J^a is defined to be the sum of the nodal errors squared as shown in Eq. (5):

$$J^a = \tfrac{1}{2}\boldsymbol{E}_s^T\boldsymbol{E}_s = \tfrac{1}{2}(\boldsymbol{Y}-\hat{\boldsymbol{Y}})^T(\boldsymbol{Y}-\hat{\boldsymbol{Y}}) \tag{5}$$

The vector of nodal errors E_s is the error of each surface node between the actual $\hat{\boldsymbol{Y}}$ and desired $\boldsymbol{Y}$ surface shape. $\hat{\boldsymbol{Y}}$ is defined in Eq. (6). The boolean weighting matrix $\boldsymbol{T}_s$ weights only those

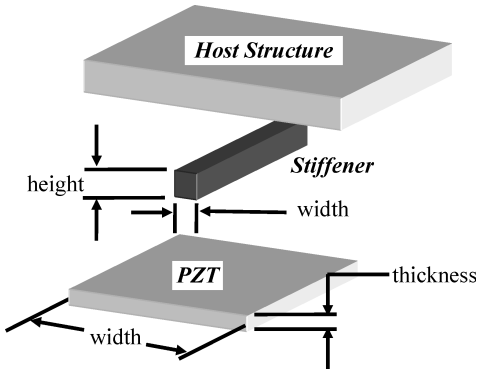

Fig. 4 Dimension definitions for active stiffener.

degrees of freedom corresponding to the vertical displacements on the surface of the host structure:

$$\hat{\boldsymbol{Y}} = \boldsymbol{T}_s\boldsymbol{K}^{-1}\boldsymbol{B}_{\mathrm{PZT}}\boldsymbol{E}_3 \tag{6}$$

The principal idea is to find a vector of electrical fields that minimizes J^a. Therefore the minimum of the quadratic function J^a is found where the gradient is equal to zero as shown in Eq. (7), and the resulting vector of optimal electrical fields is derived and shown in Eq. (8). Because the matrix $(\boldsymbol{B}_{\mathrm{pzt}}^T\boldsymbol{K}^{-T}\boldsymbol{T}_s^T\boldsymbol{T}_s\boldsymbol{K}^{-1}\boldsymbol{B}_{\mathrm{pzt}})$ is always nonnegative definite, the function J^a has a minimum, and if the matrix is nonsingular the minimum of the function is unique[10]:

$$\frac{\mathrm{d}V}{\mathrm{d}E_3} = \left(\boldsymbol{B}_{\mathrm{pzt}}^T\boldsymbol{K}^{-T}\boldsymbol{T}_s^T\boldsymbol{T}_s\boldsymbol{K}^{-1}\boldsymbol{B}_{\mathrm{pzt}}\right)\boldsymbol{E}_3 - \boldsymbol{B}_{\mathrm{pzt}}^T\boldsymbol{K}^{-T}\boldsymbol{T}_s^T\boldsymbol{Y} = 0 \tag{7}$$

$$E_3^{\mathrm{opt}} = \left(\boldsymbol{B}_{\mathrm{pzt}}^T\boldsymbol{K}^{-T}\boldsymbol{T}_s^T\boldsymbol{T}_s\boldsymbol{K}^{-1}\boldsymbol{B}_{\mathrm{pzt}}\right)^{-1}\boldsymbol{B}_{\mathrm{pzt}}^T\boldsymbol{K}^{-T}\boldsymbol{T}_s^T\boldsymbol{Y} \tag{8}$$

RMS Surface Error Calculation

For shape control, rms surface error is a commonly used performance index. To calculate the rms surface error for a continuous system, the error squared is spatially integrated over the surface of the plate as shown in Eq. (9):

$$E_{\mathrm{RMS}} = \sqrt{\frac{1}{A}\int_A (E_{\mathrm{loc}})^2\,\mathrm{d}A} \tag{9}$$

For the finite element model having many discrete elements, the following form of Eq. (9) is utilized where i is the element index number [Eq. (10)]. A three-point Gauss quadrature is used for integrating the error squared over the surface of each individual element i:

$$E_{\mathrm{RMS}} = \sqrt{\sum_{i=1}^{n_{\mathrm{el}}}\int_{A_i}\left(E_{\mathrm{loc}}^i\right)^2\,\mathrm{d}A_i \Big/ \sum_{i=1}^{n_{\mathrm{el}}} A_i} \tag{10}$$

Static Shape Control Analysis and Discussion

For planar monolithic piezoceramic actuators, the electromechanical coupling values are equal in both the x and y directions ($e_{311} = e_{322}$). These coupling parameters ultimately determine the amount of actuation that is transmitted in both the x and y directions to the host structure under an applied electrical field. For high-precision shape control, it might not always be desirable that the planar electromechanical coupling values of the piezoceramic are equal, meaning that the performance of the system could be improved with individual tailoring of the coupling parameters, or more realistically, through the design of decoupling mechanisms between the host structure and the actuator.

In the paper by Philen and Wang,[11] a detailed local analysis of a single active stiffener is presented for the understanding of the decoupling mechanism. Shown in Fig. 5 is a simple illustration

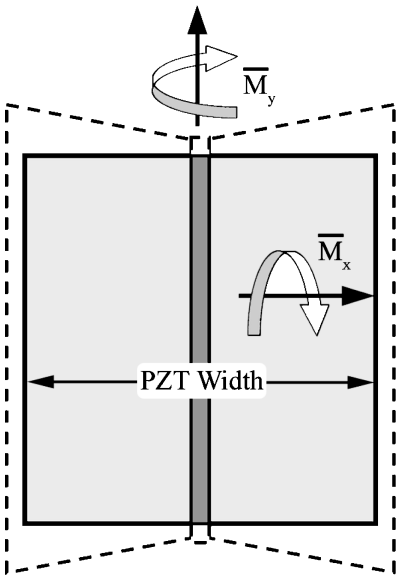

Fig. 5 Actuation illustration of active stiffener (——, original PZT configuration and – – –, actuated PZT).

of the actuation mechanism of the active stiffener, where $\bar{M}_x$ is the average moment transmitted to the host structure in the actuation direction and $\bar{M}_y$ is the average moment transmitted to the host structure in the decoupled direction. It is demonstrated in the paper[11] that through proper design of the stiffener (height, width, material selection) the average moment in the decoupled direction can be reduced to zero, which cannot be achieved with the direct attached actuator for any size or shape. It is also shown that increasing the width of the piezoelectric actuator has negligible effect on the average moment $\bar{M}_y$ (authority in decoupled direction), but can significantly increase the average moment $\bar{M}_x$ (authority in actuation direction).[11] Therefore, with the active stiffener treatment, zero average moment $\bar{M}_y$ can be achieved while maintaining significant high authority in the actuation direction. On the other hand, if one merely reduces the width of the direct attached actuator or make it the same size as that of the stiffener in the active stiffener actuator, the authority in the actuation direction will be significantly decreased and the authority in the decoupled direction will still not become zero (although it will be reduced). These analysis results clearly illustrated the merit of adding the stiffener insertion.

In this paper, the term mode is used to represent a type of static surface aberration, such as the power mode described by the Zernike polynomial. Because the Zernike polynomial function is a product of both a purely radial function and a purely angular function, the circumferential modes are defined where the radial function is monotonically increasing or decreasing and the angular (circumferential) wave number is greater than one. As seen in Fig. 3, for the system with direct attached actuators the width of the radial actuator is small in comparison to the plate circumference, and as a result the circumferential action of the radial actuator yields negligible control authority in the lower-order circumferential modes, but can cause unwanted localized deformation in the circumferential direction. Therefore, the circumferential expansion/contraction cannot provide the authority to control the lower-order circumferential modes, but reducing this action can significantly reduce the possibility of exciting the higher-order uncontrolled modes.

As mentioned, the surface error is to be represented by the Zernike polynomials, which is valid for a complete circular plate pinned at the center. To prevent numerical problems caused by large element aspect ratios using the brick elements, the finite element model (large-scale analytical model) in this analysis has an inner radius of 15.2 cm and an outer radius of 127.0 cm (Figs. 2 and 3), which results in only a 1.4% reduction in the surface area compared to a

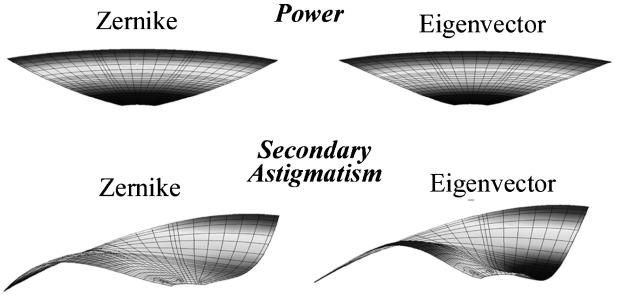

Fig. 6 Zernike polynomial and eigenvector comparison.

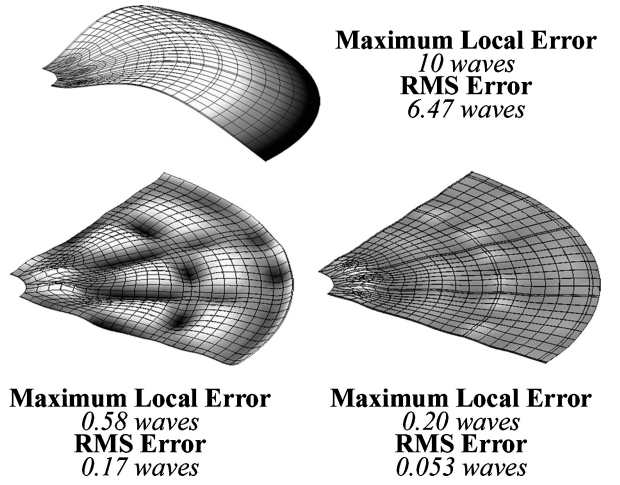

Fig. 7 Surface error for DA and AS when correcting for primary spherical mode.

complete circular plate. As a result of the prescribed boundary conditions at the inner radius, the eigenvectors of a model of only the host structure (no actuators or stiffeners) are used to represent the surface deformations. The eigenvectors for the host structure model correlate very well with the lower Zernike polynomials (Fig. 6), where the only significant difference in surface error representation arises as a result of the boundary conditions at the inner radius. Therefore the nomenclature for the Zernike polynomials (power, primary astigmatism, etc.) is applied to the host structure eigenvectors for establishing a physical understanding of the deformation type (power mode, primary astigmatism mode, etc).

By using a configuration of stiffeners sandwiched between the host structure and the actuator, it is possible to reduce the unwanted actuation and localized deformation. To demonstrate this, Figs. 7 and 8 reveal the surface error for the systems with the active stiffener and direct attached actuators when correcting for the primary spherical and secondary tetrafoil modes. Shown in the figures is the surface error of the two systems after applying the optimal electrical fields when correcting for the two deformations having an initial maximum error of 10 waves. (The wavelength used in the paper is defined to be the vacuum wavelength of a HeNe laser; 1 wavelength = 633 nm.) The optimal electrical fields are determined as calculated in Eq. (8). Basically, the structures are initially in the shape of the deformation mode only, and the objective is to activate the piezoelectric actuators such that the surface of the plate is as flat as possible. From the figures, it is apparent that the direct attached actuators generate more localized deformation in the structure between the stiffeners than that with the active stiffeners. These unwanted deformations are the higher-order modes that are being excited by the direct attached actuators, and this type of behavior is also seen when controlling the remaining modes of interest.

As demonstrated by Philen and Wang[11] for a single active stiffener attached to a flexible host structure, the height and width of the insert can dramatically affect the transmitted moment to the host structure in both the decoupled and actuation directions. Therefore, the height

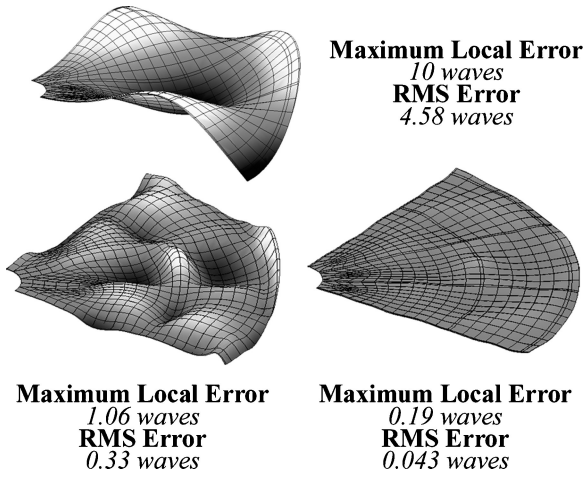

Fig. 8 Surface error for DA and AS when correcting for secondary tetrafoil mode.

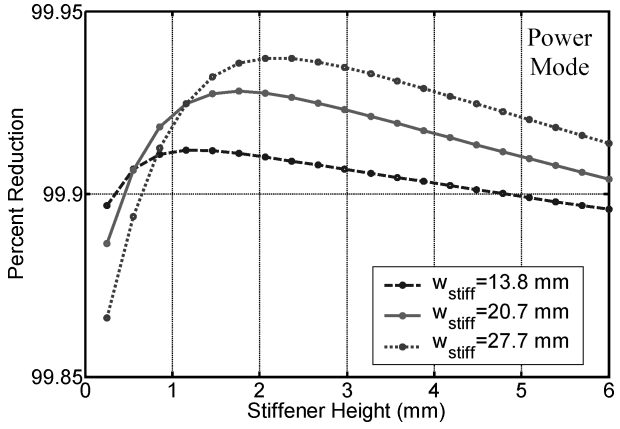

Fig. 9 Stiffener height and width effect on the rms surface error percent reduction for power mode.

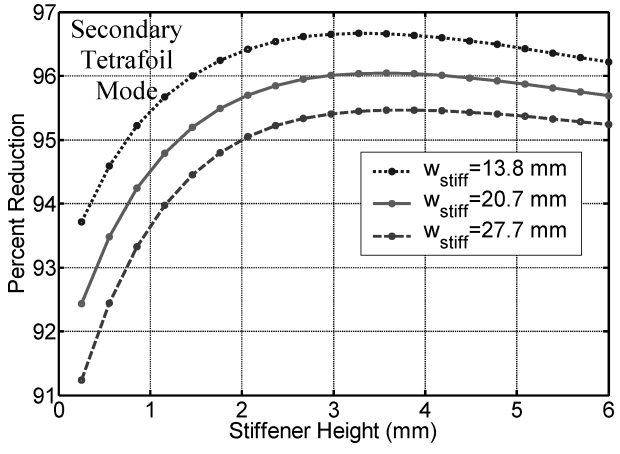

Fig. 10 Stiffener height and width effect on the rms surface error percent reduction for secondary tetrafoil mode.

and width of the stiffeners can greatly affect the performance of the plate having multiple actuators. Shown in Figs. 9 and 10 is the effect of the height and width of the stiffeners on the rms surface error percent reduction when correcting for the power and secondary tetrafoil modes. As seen in the plots, there is an optimal stiffener height for each stiffener width. With the power mode (Fig. 9), increasing the width of the stiffener slightly increases the performance with the optimal stiffener height, but it is the only deformation mode of interest that displays this behavior. All of the other deformation modes of interest demonstrate that the performance increases with decreasing stiffener width, similar to the plot for the secondary tetrafoil mode (Fig. 10). For the study, the stiffener parameters are limited within the range of values shown to prevent any numerical problems caused by large aspect ratios. For the remaining modes not shown, the 13.8-mm stiffener width (the smallest width studied) outperformed the larger stiffener widths investigated, and the optimal stiffener height occurs between 2 and 4 mm, which illustrates that a thin stiffener with a finite stiffener height can control the shape of the structure better than the direct attached actuators because none of the results suggest a zero stiffener height as optimal. Recall that the width of the piezoceramic sheets is 76.2 mm.

The designed actuator configuration has the greatest controllability over the power deformation mode (the lowest-order non-rigid-body deformation mode), and the effect of changing stiffener parameters is not as dramatic as with the higher-order modes. As the mode number increases, the effect becomes more dramatic. For example, the minimum and maximum percent reduction is 89 and 95%, respectively, for the tertiary astigmatism mode within the range of stiffener heights and widths.

For the circumferential modes (primary astigmatism, primary tetrafoil, etc.) investigated, the radial and circumferential strain throughout the structure is in directions opposite to one another. Therefore the ideal actuator for controlling these deformation modes would be one that expands in one direction while contracting in the orthogonal direction. Although the planar monolithic piezoceramic sheet actuator does not possess these properties, the active stiffener is able to increase the performance caused by the decoupling effect of the insert (stiffener). On the other hand, the radial and circumferential strain throughout the structure for the power mode is in the same direction but not equal in magnitude. As a result, the ideal actuator is one where the radial and circumferential actuation is in the same direction to one another, but not necessarily equal in magnitude. Philen and Wang[11] demonstrated that decreasing the height and increasing the width of the stiffener increases the average transmitted moment in the decoupled direction when analyzing a single active stiffener attached to a flexible host structure. Therefore, as shown in Fig. 9, with a short stiffener (height = 0.25 mm) decreasing the width of the stiffener increases the performance by reducing the authority in the decoupled direction. As one increases the height of the stiffener for a given width, the performance of the system reaches a maximum value. For a wider stiffener, then the optimal stiffener height increases. This increase in the optimal stiffener height with increasing width ensures that an optimal level of actuation authority is maintained. The remaining deformation modes of interest (secondary astigmatism, secondary tetrafoil, etc.; see Table 1 for list of deformation modes) have regions where the direction and magnitude of the circumferential and radial strains change throughout the structure, and as a result the active stiffener is able to give better overall performance than the direct attached actuator. For the remaining discussion, a stiffener width of 13.8 mm and height of 3 mm is used for the analysis.

For further insight into the decoupling ability of the active stiffener, Figs. 11 and 12 reveal the contribution of the uncontrolled modes in the surface error of the systems when correcting for the primary spherical and secondary astigmatism modes. The vertical axis is the magnitude of the modal contribution, or how much of the mode exists in the surface error. This surface error is the error in the surface after the optimal electrical fields have been applied. The horizontal axis is the mode numbers. The gray bars are for the direct attached actuators, and the black bars are for the active stiffener actuators. For the analysis, the eigenvectors for the thin circular plate model without the stiffeners and actuators are used as trial functions to reconstruct the surface error of the mirrors in order to compare the two systems having direct attached and active stiffener actuators. These trial functions are thus designated as the mode shapes (horizontal axis), and the vector containing the magnitudes for each trial function is defined as the modal magnitude vector (vertical axis). Mathematically, the nodal displacement vector describing the reconstructed surface $\tilde{\boldsymbol{Y}}$ is defined to be equal to

Table 1 RMS and maximum error percent reduction for DA and AS

Circumferential wave number			Radial wave number 2		4		6		8		10	
			Mode shape	Percent reduction	Mode shape	Percent reduction	Mode shape	Percent reduction	Mode shape	Percent reduction	Mode shape	Percent reduction
0	DA	RMS	Power	99.7	Pri spher	97.4	Sec spher	87.3	Ter spher	70.7	N/A	——
		Max	——	99.3	——	94.2	——	80.3	——	66.0	——	——
	AS	RMS	——	99.9	——	99.2	——	97.0	——	91.7	——	——
		Max	——	99.7	——	98.0	——	95.6	——	87.9	——	——
2	DA	RMS	Pri astig	98.8	Sec astig	92.8	Ter astig	81.5	Quat astig	64.1	N/A	——
		Max	——	97.4	——	89.4	——	70.5	——	54.1	——	——
	AS	RMS	——	99.8	——	99.1	——	94.3	——	88.6	——	——
		Max	——	99.7	——	98.1	——	92.1	——	80.1	——	——
4	DA	RMS	0	——	Pri tetra	96.6	Sec tetra	84.2	Ter tetra	56.1	Quad tetra	47.1
		Max	——	——	——	90.0	——	69.9	——	41.4	——	35.1
	AS	RMS	——	——	——	99.0	——	96.6	——	79.6	——	72.3
		Max	——	——	——	98.6	——	94.4	——	78.5	——	67.2
6	DA	RMS	0	——	0	——	Pri hexa	94.4	Sec hexa	86.0	Ter hexa	74.4
		Max	——	——	——	——	——	88.9	——	83.3	——	74.1
	AS	RMS	——	——	——	——	——	97.5	——	96.8	——	90.8
		Max	——	——	——	——	——	95.3	——	95.8	——	88.6
8	DA	RMS	0	——	0	——	0	——	Pri octa	89.1	Sec octa	64.2
		Max	——	——	——	——	——	——	——	80.0	——	61.1
	AS	RMS	——	——	——	——	——	——	——	95.4	——	74.2
		Max	——	——	——	——	——	——	——	94.4	——	67.0
10	DA	RMS	0	——	0	——	0	——	0	——	Pri deca	85.3
		Max	——	——	——	——	——	——	——	——	——	77.2
	AS	RMS	——	——	——	——	——	——	——	——	——	92.9
		Max	——	——	——	——	——	——	——	——	——	90.2

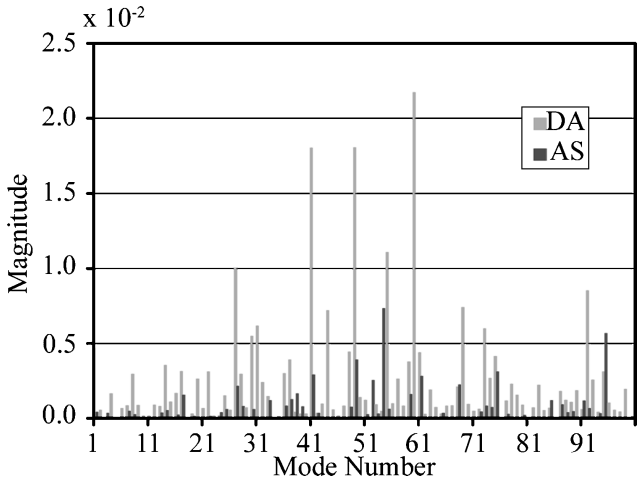

Fig. 11 Higher modal excitation for DA and AS when correcting for primary spherical mode.

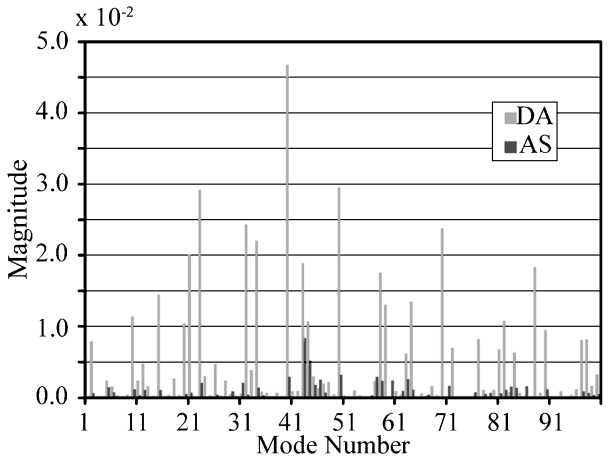

Fig. 12 Higher modal excitation for DA and AS when correcting for secondary astigmatism mode.

the matrix of trial functions Φ_0 multiplied by the modal magnitude vector η as shown in Eq. (11). The vector of nodal displacements describing the deformed surface is designated as $\hat{Y}$ in Eq. (6). To determine the vector of magnitudes for the trial functions that best reconstruct the surface error, a least-squares problem is formulated where J^t in Eq. (12) is minimized with respect to η after Eq. (11) is substituted into Eq. (12). The modal magnitude vector can be solved for as shown in Eq. (13), and this is the value used in the figure for both systems:

$$\tilde{Y} = \Phi_0 \eta \tag{11}$$

$$J^t = \tfrac{1}{2}(\hat{Y} - \tilde{Y})^T(\hat{Y} - \tilde{Y}) \tag{12}$$

$$\eta^{\mathrm{OPT}} = \left(\Phi_0^T \Phi_0\right)^{-1} \Phi_0^T \hat{Y} \tag{13}$$

For the analysis, the initial maximum deformation of the plate has been normalized to a value of one, and the maximum value for each of the 100 trial functions has been normalized to a value of one. For example, when using Fig. 11, if the plate for the system with direct attached actuators has an initial deformation in the form of the primary spherical mode with a maximum value of 10 waves, then mode number 41 exists in the surface error with a maximum value of 0.018×10 waves.

As seen in the two figures, the direct attached actuators consistently excite these higher modes (initially all at zero initial condition) more so than the active stiffener actuators when correcting for the two deformations. Although the normalized modal magnitudes of the higher order modes are smaller than one, reducing the magnitude as much as possible is crucial when trying to achieve a high-precision surface shape. This behavior is also seen when controlling the remaining modes.

Table 2 Maximum electrical fields for DA and AS (maximum initial error 10 waves)

Mode	DA, V/mm	AS, V/mm
Pri astig	6.2	1.6
Power	2.8	2.6
Pri tetra	13.0	6.9
Pri spher	15.8	14.0
Pri hexa	18.4	11.0
Sec astig	17.0	18.6
Pri octa	31.1	35.1
Sec tetra	36.4	41.7
Ter astig	61.7	44.3
Pri deca	34.5	56.9
Sec spher	40.3	46.2
Sec octa	45.6	109.6
Sec hexa	29.5	46.6
Ter tetra	65.5	95.7
Quad astig	90.4	111.8
Ter spher	68.5	89.0
Quad tetra	109.8	195.0
Ter hexa	56.8	126.0

Table 1 illustrates the performance of both the direct attached and the active stiffener actuators when correcting for the lower-order modes. Shown in the table for each mode shape are the radial and circumferential wave number corresponding to the Zernike polynomial representations and the rms surface error and maximum error percent reduction for both the direct attached and active stiffener actuators. As seen in the table, it is evident that significant reductions in the surface error can be achieved, and more importantly the active stiffener actuators are able to correct for more error than the direct attached actuators for all of the mode shapes shown. Also as seen in the table, the performance improvement of the active stiffener over the direct attached actuator increases as the mode order increases.

Shown in Table 2 are the maximum electrical field values for the two systems when correcting for each mode having an initial maximum error of 10 waves. As seen, the active stiffener actuators require less control voltage than the direct attached actuators for six of the 18 modes and require more voltage for the remaining modes. Recall that the study compares the maximum performance of each system, and no limits are placed upon the voltages because we are interested in achieving the maximum possible performance for high-precision shape control. Also the maximum electrical fields are below 200 V/mm and therefore are far from the operating limit of 500 V/mm.

Experimental Investigation

To experimentally evaluate the active stiffener actuator for shape control, two adaptive flexible plates are manufactured. The first plate has piezoelectric ceramic actuators directly attached to the back of the plate, and the second plate utilizes the active stiffeners. The host structure for both systems is half of a circular 12-in. (305-mm)-diam plate having a thickness of 1/16 in. (1.59 mm) and is machined from aluminum 5052 having a reflective finish on the front. The plates are cantilevered along the edge as illustrated in Fig. 13 using a 2.5×2 in. (63.5×50.8 mm) aluminum 6061 bar.

Both of the adaptive plates have six piezoelectric actuators (American Piezo Ceramics, Inc., APC-850), where each actuator has a length of 2.5 in. (63.5 mm), width of 0.5 in. (12.7 mm), and a thickness of 0.04 in. (1 mm). For the first plate, the piezoceramic patches are directly bonded to the back of the plate using high-strength epoxy. As seen in Fig. 13, the six actuators are placed in three radial lines with two actuators per radial line. The stiffeners (inserts) used for the active stiffeners for the second plate are machined from aluminum 6061 having a length of 5 in. (127 mm), width of 0.2 in. (5.1 mm), and a height of 1/8 in. (3.18 mm) (Fig. 13). There are three radial stiffeners, each having two piezoceramic patches bonded to the surface using high-strength epoxy. The active stiffeners are bonded to the back of the plate using high-strength epoxy in the same configuration as the first plate. To verify the analytical modeling technique and procedure presented in the preceding sections, finite element models of these test plates (defined to be the small-scale analytical models) are developed and analyzed using the same approach described in preceding sections on the large-scale model (shown in Fig. 13 to the right of the experimental plates).

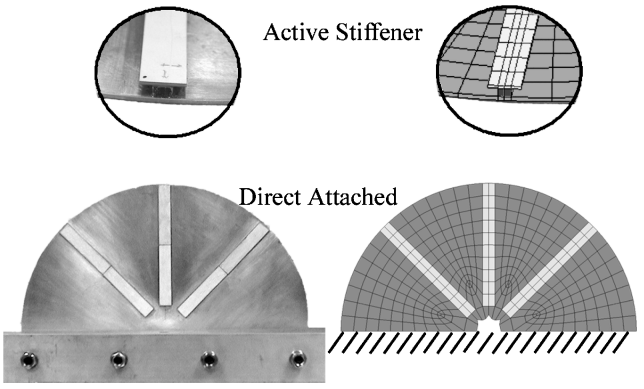

Fig. 13 Experimental plate specimens and corresponding analytical models with direct attached and active stiffener actuators.

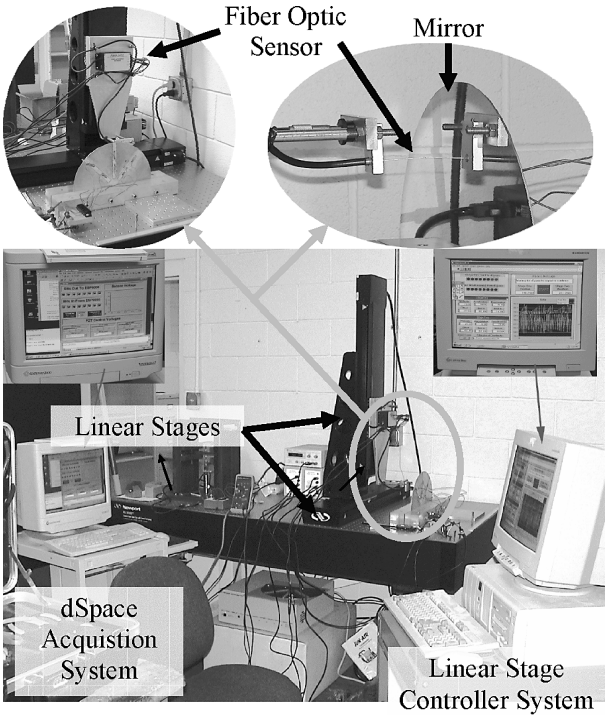

Fig. 14 Configuration of experiment.

For performing the experiment, the adaptive plates are attached to a Newport RS3000 tuned isolation table (Fig. 14). The surface displacements of the plates are measured using a Philtec D20 fiber-optic sensor mounted to two Newport IMS-500 high-performance linear stages giving both horizontal and vertical motion. The motorized stages are controlled using a two-channel motion controller (Newport ESP-6000) through LabView instrumentation software. A dSpace acquisition system is used to record the surface displacements from the fiber-optic sensor and to actuate the piezoelectric actuators in conjunction with PCB Piezotronic amplifiers. Communication between the dSpace system and linear stage controller system is accomplished through digital I/O lines, thereby automating the testing process.

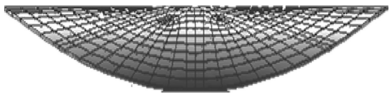

Fig. 15a Initial rms surface error: 3.92; initial maximum error: 10.00.

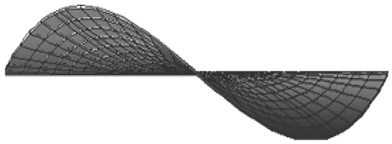

Fig. 15b Initial rms surface error: 3.79; initial maximum error: 10.00.

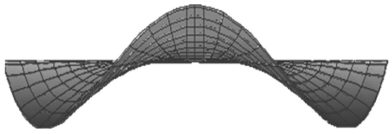

Fig. 15c Initial rms surface error: 3.42; initial maximum error: 10.00.

For the experiment, the plates are assumed to be flat, and the goal is to deform the plates in the shape of predetermined shapes. In the experiment, only the displacements on the surface of the plates are measured, which is accomplished by subtracting the baseline (controller off) measured plate shape from the actuated (controller on) measured plate shape. The surface error is determined by subtracting the actual profile from the desired surface profile. The desired profiles are determined to emulate the lower Zernike polynomials. (Mathematically are the eigenvectors obtained from the small-scale analytical models of the 12-in.-diam cantilevered mirror without any stiffeners and actuators.) Although the plates are cantilevered, the eigenvectors resemble those of the Zernike polynomials as seen in Fig. 15, where the shown desired shape is similar to the primary tetrafoil.

For determining the optimal voltages used in the experiment, a series of preliminary tests are performed to determine each actuator's influence on the surface shape. Although there are six piezoelectric actuators on each plate, the actuators arranged along the radial lines are actuated with equivalent voltages, thereby essentially treating the two actuators along radial lines as one actuator. For the experiment, there are a total of 1013 measurement locations on the surface, which correspond to the surface nodal locations in the small-scale analytical models. For every measurement point, the voltage from the fiber-optic sensor is recorded as each actuator is turned on and off individually using a voltage of 140 V. After recording the sensor signals for all of the measurement locations, the relative surface displacements ($\hat{\boldsymbol{Y}}_1^{140V}$, $\hat{\boldsymbol{Y}}_2^{140V}$, $\hat{\boldsymbol{Y}}_3^{140V}$) can be determined for each of the three actuators. Subsequently three nodal-voltage influence vectors (φ_{PZT1}, φ_{PZT2}, φ_{PZT3}) can be calculated, which determines how the surface of the plate displaces by a voltage applied to each actuator as seen in Eq. (14):

$$\{\varphi_{\mathrm{PZT1}}\} = \frac{\left\{\hat{\boldsymbol{Y}}_1^{140V}\right\}}{140\,\mathrm{V}}, \qquad \{\varphi_{\mathrm{PZT2}}\} = \frac{\left\{\hat{\boldsymbol{Y}}_2^{140V}\right\}}{140\,\mathrm{V}}$$

$$\{\varphi_{\mathrm{PZT3}}\} = \frac{\left\{\hat{\boldsymbol{Y}}_3^{140V}\right\}}{140\,\mathrm{V}} \tag{14}$$

Using the three nodal-voltage influence vectors, a nodal-voltage influence matrix $\boldsymbol{\Phi}_{\mathrm{PZT}}$ can be assembled, which relates the displacement of the surface nodes $\hat{\boldsymbol{Y}}$ to the voltage applied across the piezoelectric actuators $\boldsymbol{V}_{\mathrm{PZT}}$ as shown in Eq. (15):

$$\{\hat{\boldsymbol{Y}}\} = [\{\varphi_{\mathrm{PZT1}}\} \quad \{\varphi_{\mathrm{PZT2}}\} \quad \{\varphi_{\mathrm{PZT3}}\}] \begin{Bmatrix} \boldsymbol{V}_{\mathrm{PZT1}} \\ \boldsymbol{V}_{\mathrm{PZT2}} \\ \boldsymbol{V}_{\mathrm{PZT3}} \end{Bmatrix} = \boldsymbol{\Phi}_{\mathrm{PTZ}} \boldsymbol{V}_{\mathrm{PZT}} \tag{15}$$

Table 3 Experimental and analytical rms and max error results for AS and DA (units: micrometers)

	Analytical results		Experimental results	
Actuator	Final rms error	Maximum error	Final rms error	Maximum error
DA	1.27	3.97	1.39	3.19
AS	1.28	4.18	1.31	4.25
DA	1.99	4.63	1.96	3.16
AS	0.99	2.62	1.01	2.80
DA	2.94	6.35	2.89	3.52
AS	0.88	1.79	0.94	2.58

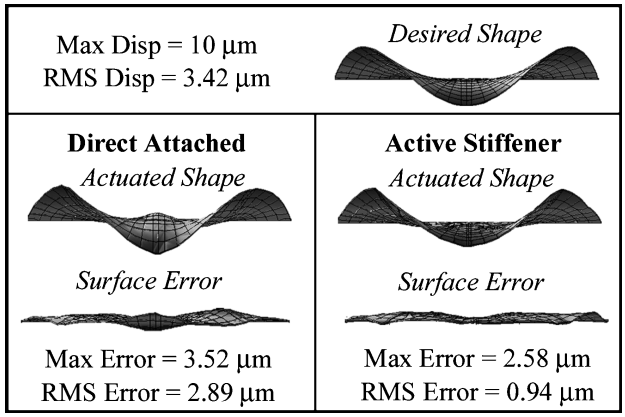

Fig. 16 Experimental results for third mode.

After determining the matrix $\boldsymbol{\Phi}_{\mathrm{PZT}}$, the experimentally determined optimal voltages for shape control can be determined using a least-squares approach similar to the method illustrated in the mathematical formulation section by minimizing the objective function shown in Eq. (16). The vector of optimal voltages is shown in Eq. (17), where $\boldsymbol{V}_{\mathrm{PZT}}^{\mathrm{OPT}}$ is the vector of optimal voltages and $\boldsymbol{Y}$ is the vector of desired displacements on the surface of the plate:

$$J^e = \tfrac{1}{2}\boldsymbol{E}_s^T\boldsymbol{E}_s = \tfrac{1}{2}(\boldsymbol{Y} - \boldsymbol{\Phi}_{\mathrm{PZT}}\boldsymbol{V}_{\mathrm{PZT}})^T(\boldsymbol{Y} - \boldsymbol{\Phi}_{\mathrm{PZT}}\boldsymbol{V}_{\mathrm{PZT}}) \tag{16}$$

$$V_{\mathrm{PZT}}^{\mathrm{OPT}} = \left(\boldsymbol{\Phi}_{\mathrm{PZT}}^T\boldsymbol{\Phi}_{\mathrm{PZT}}\right)^{-1}\boldsymbol{\Phi}_{\mathrm{PZT}}^T\boldsymbol{Y} \tag{17}$$

After determining optimal voltages, the experiment is repeated where the actuators are simultaneously actuated using the optimal voltages, and the surface displacements are measured for each location before and after actuation. The method in Eqs. (14–17) assumes that the physical system is linear, and the method of superposition can be applied, thus suggesting that simultaneously actuating multiple actuators is equivalent to individually actuating each actuator with the calculated voltage and summing the displacements. This process of determining the optimal voltages is considered valid because there is less than a 2% difference in the rms surface area displacement when using Eq. (15) with the calculated optimal voltages and when repeating the experiment using the calculated optimal voltages (simultaneous actuation).

Shown in Table 3 are the rms surface error and maximum error values for the first three low-order modes (shown in Figs. 15a–15c). The column labeled Analytical Results shows the results acquired from evaluation of the small-scale analytical models using the optimal voltages determined from Eq. (8), and the column labeled Experimental Results shows the results obtained by performing the experiment using the optimal voltages determined by Eq. (17).

As seen in the table, there is good agreement between the analytical and the experimental results (rms surface error and maximum

error) for the active stiffener and direct attached actuators for all three mode shapes. The only more noticeable discrepancy is on the maximum surface error value in the third mode shape for the direct attached actuator. This is most likely caused by yielding of the bonding layer between the actuator and the host structure. Because the bonding layer is not considered in the analytical model, the direct attached actuator performs better in the experiment than analytically predicted because of the reduction of coupling between the host structure and actuator in the circumferential direction caused by the bonding layer. This phenomenon is more significant for higher-order modes because as the circumferential mode number increases the circumferential strain in the host structure increases for the same specified maximum displacement; and thus the system performance is more sensitive to the actuator-structure coupling in the circumferential direction. Nevertheless, the analytical results possess the same overall trend as observed in the experiment, where the performances of the two actuation systems are close for the first mode and the performance of the active stiffener actuator over the direct attached actuator increases as the mode number increases. This agreement between the analysis and the experiment further enhances the validity of the findings obtained from the large-scale analytical models because the model formulation and control methodology for the small-scale and large-scale analytical models are identical.

Closer examination of the third shape (Fig. 16) further illustrates the advantage of the active stiffener over the direct attached actuator. For the shape shown at the top of the figure, the experimental results for the test system demonstrate that the active stiffeners can control the shape of the mirror better than the direct attached actuators. The surface error plot for the system with the active stiffeners reveals a reduced wrinkling effect than the system with the direct attached actuators as a result of the decoupling ability of the stiffener. Such observations verify the trend predicted by the analysis results obtained from the large-scale and small-scale analytical models.

Conclusions

The focus of this research is on surface control of optical mirrors. The configuration of active stiffeners placed in the radial and circumferential line directions of a circular plate (host structure of the mirror) is chosen as actuators to control the mirror. The purpose of this study is to investigate the feasibility of the active stiffener for attaining a high-precision surface through utilizing the stiffeners' directional decoupling mechanism. The analytical results demonstrate that the active stiffener can achieve significant reductions in surface error for all of the deformation modes of interest and outperforms the direct attached actuator. The experimental results also illustrate the performance improvement of the active stiffener concept over the direct attached actuator and verify the trend observed in the analytical results.

Appendix: Analytical System Parameters

Table A1 Analytical system parameters

Description	Value
Circular plate	
Material	ULE Glass
Modulus, N/m^2	$6.70E+10$
Poisson	0.17
Density, kg/m^3	$2.20E+03$
Radius, m	1.27
Thickness: DA system, mm	4.1
Thickness: AS system, mm	3.68

(**Continued**)

Table A1 Analytical system parameters (continued)

Description	Value
Stiffener	
Modulus, N/m^2	$7.10E+10$
Poisson	0.33
Density, kg/m^3	$2.76E+03$
Width, mm	13.8
Thickness, mm	3
Actuator	
Type	PZT-4
Number/radial line	6
Number/circumferential line	9
Thickness, mm	0.5
Density, kg/m^3	$7.50E+03$
Stiffness parameters, N/m^2	Orthotropic
D1111	$1.05E+11$
D1122	$5.53E+10$
D1133	$5.73E+10$
D2222	$1.05E+11$
D2233	$5.73E+10$
D3333	$9.65E+10$
D1212	$1.91E+10$
D1313	$1.91E+10$
D2323	$2.50E+10$
Electromechanical coupling, N · m · V	
e311	−3.19155
e322	−3.19155
e333	23.367
e312, e323, e313	0

Acknowledgment

This research is sponsored by the Eastman Kodak Company.

References

[1]Wagner, J. W., Agnes, G. S., and Magee, E., "Optical Metrology of Adaptive Membrane Mirrors," *Journal of Intelligent Material Systems and Structures*, Vol. 11, No. 11, 2000, pp. 837–847.

[2]Agnes, G. S., and Wagner, J. W., "Adaptive Structures Technology for Membrane Optical Surfaces," *Collection of Technical Papers—AIAA/ASME/ASCE/AHS/ASC Structures, Structural Dynamics, and Materials Conference*, Vol. 1, AIAA, Reston, VA, 2001, pp. 170–175.

[3]Kuo, C.-P., and Bruno, R., "Optimal Actuator Placement on an Active Reflector Using a Modified Simulated Annealing Technique," *US/Japan Conference on Adaptive Structures*, Technomic, Lancaster, PA, 1990, pp. 1056–1067.

[4]Liu, C. H., Hagood, N. W., and Hall, E. K., "Adaptive Lightweight Mirrors for the Correction of Self-Weight and Thermal Deformations," *ASME Adaptive Structures and Materials Systems*, Vol. AD-35, American Society of Mechanical Engineers, 1993, pp. 171–183.

[5]Kapania, R., Mohan, P., and Jakubowski, A., "Control of Thermal Deformations of Spherical Mirror Segment," *Journal of Spacecraft and Rockets*, Vol. 35, No. 2, 1998, pp. 156–162.

[6]Philen, M. K., and Wang, K. W., "Shape Control of Circular Plate with Piezoelectric Sheet Actuators," *Proceedings of the SPIE*, Vol. 4327, Society of Photo-Optical Instrumentation Engineers, Bellingham, WA, 2001, pp. 709–719.

[7]Birman, V., Knowles, G. J., and Murray, J. J., "Application of Piezoelectric Actuators to Active Control of Composite Spherical Caps," *Smart Materials and Structures*, Vol. 8, No. 2, 1999, pp. 218–222.

[8]Birman, V., Griffin, S., and Knowles, G., "Axisymmetric Dynamics of Composite Spherical Shells with Active Piezoelectric/Composite Stiffeners," *Acta Mechanica*, Vol. 141, No. 1, 2000, pp. 71–83.

[9]Cook, R., Malkus, D., and Plesha, M., *Concepts and Applications of Finite Element Analysis*, J. Wiley, New York, 1989, Chap. 6.

[10]Astrom, K. J., and Wittenmark, B., *Adaptive Control*, Addison Wesley Longman, Reading, MA, 1995, Chap. 2.

[11]Philen, M. K., and Wang, K.-W., "On the Directional Decoupling Characteristics of Active Stiffeners for Shape Control of Two-Dimensional Structures," *Smart Materials and Structures*, Vol. 13, No. 2, 2004, pp. 355–363.

B. Sankar
Associate Editor